SLAC–PUB–7898
July 1998

Bunch-Length and Beam-Timing Monitors in the SLC Final Focus*

F. Zimmermann, G. Yocky, D.H. Whittum, M. Seidel†,
C.K. Ng, D. McCormick, K.L.F. Bane

Stanford Linear Accelerator Center
Stanford University, Stanford, CA 94309, USA

During the 1997/98 luminosity run of the Stanford Linear Collider (SLC), two novel RF-based detectors were brought into operation, in order to monitor the interaction-point (IP) bunch lengths and fluctuations in the relative arrival time of the two colliding beams. Both bunch length and timing can strongly affect the SLC luminosity and had not been monitored in previous years. The two new detectors utilize a broad-band microwave signal, which is excited by the beam through a ceramic gap in the final-focus beam pipe and transported outside of the beamline vault by a 160-ft long X-Band waveguide. We describe the estimated luminosity reduction due to bunch-length drift and IP timing fluctuation, the monitor layout, the expected responses and signal levels, calibration measurements, and beam observations.

Presented at the
8th Workshop on Advanced Accelerator Concepts
Baltimore, Maryland, July 5–11, 1998

*Work supported by the U.S. Department of Energy, contract DE–AC03–76SF00515.
†present address: DESY, Notkestraße 85, D-22603 Hamburg, Germany

Bunch-Length and Beam-Timing Monitors in the SLC Final Focus[1]

F. Zimmermann, G. Yocky, D.H. Whittum, M. Seidel[2],
C.K. Ng, D. McCormick, K.L.F. Bane

Stanford Linear Accelerator Center
Stanford University, Stanford, California 94309

Abstract. During the 1997/98 luminosity run of the Stanford Linear Collider (SLC), two novel RF-based detectors were brought into operation, in order to monitor the interaction-point (IP) bunch lengths and fluctuations in the relative arrival time of the two colliding beams. Both bunch length and timing can strongly affect the SLC luminosity and had not been monitored in previous years. The two new detectors utilize a broad-band microwave signal, which is excited by the beam through a ceramic gap in the final-focus beam pipe and transported outside of the beamline vault by a 160-ft long X-Band waveguide. We describe the estimated luminosity reduction due to bunch-length drift and IP timing fluctuation, the monitor layout, the expected responses and signal levels, calibration measurements, and beam observations.

MOTIVATION

At the SLC, the IP bunch length is sensitive to many variables, most notably the injection time into the linac, the voltage of the bunch compressor RF between damping ring and linac, the R_{56} value of the ring-to-linac transport line (RTL), the longitudinal bunch distribution at extraction from the damping ring and the bunch charge. Because of hourglass effect (depth of focus) and disruption (mutual contraction of the two beams during the collision), the bunch length at the interaction point can strongly affect the luminosity. Also the beamstrahlung (synchrotron radiation in the field of the opposing beam) depends on the bunch length. We have simulated the dependence of beamstrahlung and luminosity on the bunch length using the code Guinea-Pig [2], for typical 1997 SLC parameters: bunch population $N_b \approx 3.5 \times 10^{10}$, rms beam sizes $\sigma_{x,y} \approx 1.70, 0.92$ μm, rms divergences $\theta_{x,y} \approx 460, 260$ μrad, and considering realistic (non-Gaussian) longitudinal distributions. For rms bunch lengths between 0.8 mm and 1.6 mm, the simulation results are summarized by the fitted dependences: $H_D \approx 1.0 + 0.29 \times \sigma_z$ [mm] and

---

[2] present address: DESY, Notkestr. 85, Hamburg, Germany

[1] Work supported by the U.S. Department of Energy under contract DE-AC03-76SF00515.

$\delta_B[10^{-3}] \approx 0.8 - 0.27 \times \sigma_z$ [mm], where H_D is the luminosity enhancement factor [1] and δ_B the relative energy loss due to beamstrahlung.

Hitherto, beam timing at the IP was not monitored at all. Yet it is a critical factor for IP spot-size tuning, spot-size stability and the luminosity. If the collision point shifts in time, it will no longer coincide with the beam waists, implying a non-optimum IP spot size. There are many potential sources of IP timing drifts and timing jitter, such as changes in the extraction time from the damping rings, variation of the bunch-compressor RF phase relative to the damping-ring phase, and beam energy and profile fluctuation in the linac. Diurnal timing changes, even if they are large and different for both beams, are not thought to be a problem, as the four beam waists are scanned and corrected regularly. However, changes on shorter time scales—such as pulse-to-pulse variation ('jitter') or drifts over a few minutes—could seriously degrade the average luminosity. The luminosity reduction caused by an rms timing fluctuation of Δt is roughly given by $L/L_0 \approx (1 + (c\ \Delta t/(2\beta_x^*)^2)^{-1/2}(1 + \left(c\ \Delta t/2\beta_y^*\right)^2)^{-1/2}$, where L denotes the actual luminosity, L_0 the luminosity without timing errors, c the speed of light, and β_x^*, β_y^* the nominal IP beta functions ($\beta_x^* \approx 2.8$ mm, and $\beta_y^* \approx 1.5$ mm). An rms timing jitter of 6° X-Band then corresponds to a luminosity loss of about 1.5%, and a beam-timing monitor (BTM) with a resolution of 15° X-Band (5° S-Band) could detect fluctuations resulting in a 10% luminosity loss.

BUNCH-LENGTH MONITOR

During the 1996/97 SLC downtime a novel RF bunch length monitor (BLM) was installed in the South Final Focus, about 45 m away from the IP. The monitor detects the longitudinal frequency spectrum of both electron and positron bunches, which pass this point with a time separation of roughly 300 ns. Previous attempts to commission a bunch-length monitor based on an RF cavity [3] at the same location failed, presumably because the crystal rectifiers and amplifiers used for RF-signal conversion could not withstand the high radiation and electromagnetic noise level in the final-focus tunnel.

Performing the RF conversion outside of the beamline vault overcomes the suspected noise problem and, in addition, affords easy access to the signal processor during SLC operation. For this reason, we installed a 160-ft long section of WR90 (brass) waveguide, extending from the South final-focus tunnel through a 60-ft deep ventilation shaft to the 'laser shack' South of the collider hall, where the signal is processed. The reasons for choosing overmoded rectangular WR90 (X-band) waveguide were twofold: (1) X-band components are easily available at SLAC, and (2) the waveguide attenuation is small compared with that in waveguides of higher-cutoff frequency, an important consideration for a 50-m length. Figure 1 (left) compares the attenuation in standard rectangular brass waveguides of various dimensions.

Figure 2 shows how, using waveguide filters and couplers, the RF signal is finally split into 4 different channels, which span the 4 frequency ranges 8–11.6 GHz, 11.6–

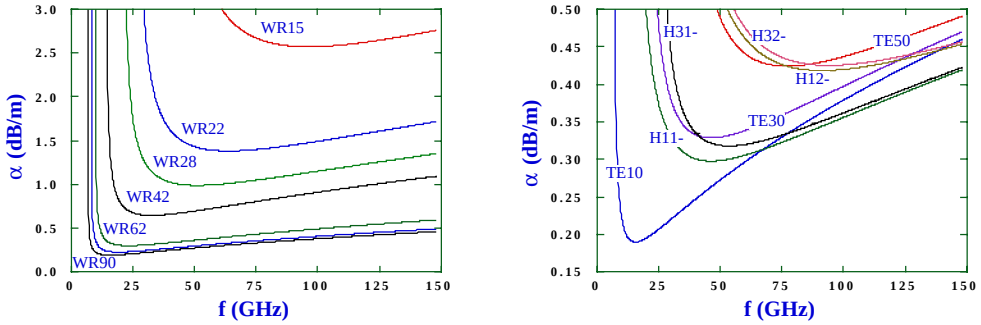

FIGURE 1. Left: TE_{10} mode attenuation in brass waveguide of standard dimensions. At low frequencies, the microwave signal propagates more slowly in the waveguide, dissipating itself in the conductor. At high frequencies the surface resistance increases. Right: attenuation vs. frequency for the lowest-order modes of WR90 waveguide coupling to the gap. The '−' sign refers to the less attenuated of a pair of degenerate hybrid modes.

19 GHz, ≥21 GHz and ≥59 GHz. The RF power in each channel is measured with crystal rectifiers connected to gated analog-to-digital converters (GADCs), and the 8 signals so obtained (4 each for both the electron and the positron beam) are continually read out by the SLC control system. The figure also shows a photograph of the signal-processing unit assembly. Multiple channels were employed since there was no confidence in the actual value of σ_z.

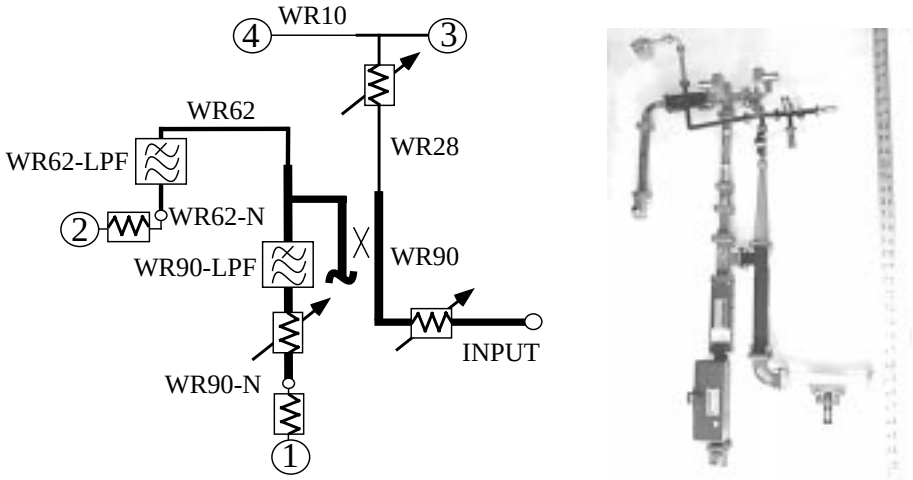

FIGURE 2. Schematic of RF signal processing (left) and photograph of assembly (right).

The frequency spectrum of a Gaussian charge distribution with rms length σ_z and total charge Q_b, moving at the speed of light, is

$$\tilde{I}_b(\omega) = \frac{Q_b}{\sqrt{2\pi}} \exp\left(-\frac{\omega^2\sigma_z^2}{2c^2}\right) \qquad (1)$$

The power radiated by the beam into an rf pick up is proportional to the square of $\tilde{I}_b$. The principle behind an rf BLM is that the sampled beam frequency spectrum,

when normalized by the square of the beam charge, correlates with the bunch length. As an example, for a 1-mm bunch length the radiated power decreases by $1/e$ at a frequency of $f = c/(2\pi\sigma_z) \approx 50$ GHz. For a 2-mm bunch length the $1/e$ fall-off would occur at 25 GHz.

In the final-focus tunnel, the open-ended WR90 waveguide is pointed at a ceramic gap in the beam pipe; see photograph in Fig. 3. This broadband pickup is more versatile than a narrow-band cavity. Inner and outer radius of the ceramic are 1.5 cm and 1.9 cm, respectively. The total gap length g is 4 cm, three quarters of which are occupied by a toroid. The waveguide is situated at the last free quarter of the gap and ends about 0.5 cm above the ceramic.

The energy radiated by the beam into the waveguide can be estimated as follows. For short bunches, $\sigma_z \ll R$ (with R the beam pipe radius), the energy loss ΔE of a bunch passing a gap is given by the diffraction model [4,5] as $\Delta E \approx 1/\pi, (1/4)Q_b^2 Z_0 c/(4\pi R)\sqrt{g/(\pi\sigma_z)}$, and corresponds to a loss factor of 3 V/pC. About half of the diffracted energy goes through the gap, the other half propagates down the beam pipe. To estimate the power radiated into the waveguide, we further must take into account the fractions of gap length (25%) and of solid angle (5%) occupied by the waveguide aperture. We then find that a 5 nC beam radiates about 0.75 μJ onto the pick up. Since this occurs in a transit time $g/c \approx 33$ ps, the peak power incident on the waveguide is about 22 kW or 73 dBm. Attenuation over 50 m will reduce this figure to 55–65 dB. Since much of this signal is at lower frequencies, where the sensitivity to bunch length is weak, the signal is filtered in frequency. Though filtering and the effect of dispersion in the waveguide will further reduce the power level, there remains sufficient peak power above 20 GHz to produce 100 mV-level signals on a commercial crystal detector (this requires only about 100 μW power), in a passive mode without amplification.

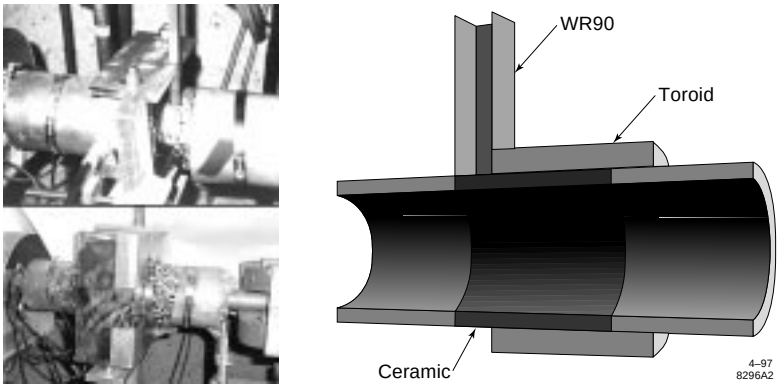

FIGURE 3. Left: photograph of waveguide pickup facing the ceramic gap (top picture), and final pick-up assembly with shielding box (bottom picture). Right: model for the numerical calculation of beam-waveguide coupling.

We used MAFIA [6] to more precisely calculate the waveguide excitation, for Gaussian bunches of different rms lengths. Figure 3 (right) depicts the model of the beam-pipe geometry used in these calculations. The 0.5-cm wide gap between

waveguide and ceramic is neglected, and the waveguide directly borders on the ceramic. The toroid is treated as a conducting boundary. The calculations show that the energy coupled into the TE_{10} mode is at least 2 times larger than that transmitted into the next important mode. Power levels at the waveguide entrance are of the order of 17–44 dBm, depending on frequency.

The interior broad dimension of the WR90 waveguide is $a = 2.286$ cm. This corresponds to a cutoff frequency $f_c = c/(2a) = 6.6$ GHz for the lowest (TE_{10}) mode. Using the skin depth $\delta_s \approx (2/(\omega\mu\sigma))^{1/2} \approx 4\mu\mathrm{m}/\sqrt{f(\mathrm{GHz})}$, where σ denotes the conductivity and the numerical value applies to brass, the surface resistance is given by $R_s = 1/(\sigma\delta_s) \approx 15\ \mathrm{m}\Omega\ \sqrt{f(\mathrm{GHz})}$. As the RF wave propagates through the waveguide, the power decreases exponentially from its initial value $P(0)$. After a distance s, the power in the TE_{10} mode is $P(s) = P(0)\exp(-2\alpha s)$, with an attenuation coefficient [7] $\alpha = R_s(2b\beta_c^2 + a\beta_0^2)/(ab\beta_0\beta_z Z_0)$, where $Z_0 = 377\ \Omega$, $b \approx a/2$ the small waveguide dimension, $\beta_c = \pi/a$, $\beta_0 = \omega/c$, and $\beta_z = (\beta_0^2 - \beta_c^2)^{1/2}$. The attenuation in dB per meter is plotted in Fig. 1 (right) for the lowest modes. There are three complications. At frequencies where the skin depth becomes comparable to the (unknown) surface roughness these formulae cease to be valid [7]. Second, there are about 41 waveguide modes with a cutoff frequency below 50 GHz, and the waveguide contains several H and E bends, at which part of the energy in the TE_{10} mode could be converted into other modes as the RF wave travels along the waveguide. Finally, in an overmoded waveguide, degenerate modes (TE_{nm} and TM_{nm} modes with the same n and m) are coupled by wall currents in the presence of attenuation, where symmetry permits [8], giving rise to hybrid modes.

The attenuation measured at 10 GHz is about 7 dB for a wave propagating twice through the entire waveguide, or about 0.2 dB per meter. This agrees well with the theoretical prediction for the waveguide attenuation due to surface resistivity. Also accounting for the 3 couplers in the signal processing unit, we can estimate the signal level at the crystal rectifiers. For the four BLM channels, these estimates are in the range 4–27 dBm, many 10's of dB above the noise. This provides a large safety margin for additional attenuation, which might arise from mode conversion or surface roughness.

For more accurate modeling, the power flow P in a single waveguide mode (index a) after a distance L can be expressed as the product of an effective voltage and current, $P_a(L,t) = V_a(L,t)I_a(L,t)$, where the current and voltage represent integrals over frequency of the beam spectrum multiplied by various transfer functions:

$$V_a(L,t) = \int_{-\infty}^{\infty} \frac{d\omega}{\sqrt{2\pi}}\ e^{j\omega t}\tilde{I}_b(\omega)\ R_a(\omega)\ F(\omega)e^{-L\{j\beta_a(\omega)+\alpha(\omega)\}} \tag{2}$$

$$I_a(L,t) = \int_{-\infty}^{\infty} \frac{d\omega}{\sqrt{2\pi}}\ e^{j\omega t}\tilde{I}_b(\omega)\ \frac{R_a(\omega)}{Z_{ca}(\omega)}\ F(\omega)e^{-L\{j\beta_a(\omega)+\alpha(\omega)\}} \tag{3}$$

Here, $\tilde{I}_b$ is the beam frequency spectrum of Eq. (1), the last exponential factor describes the propagation and attenuation through the waveguide (in the case of the TE_{10} mode, $\alpha_a = \alpha$ and $\beta_a = \beta_z$, from above), the function $F(\omega)$ is a filter which

approximates the bandpass charcateristics of the different channels in our signal processing unit, Z_{ca} is the mode impedance ($Z_{ca} = Z_0\beta_0/\beta_a$ for TE modes, $Z_{ca} = Z_0\beta_a/\beta_0$ for TM modes), and $R_a(\omega)$, in units of Ohms, represents the coupling of the beam to waveguide mode a. At low frequencies the coupling for the TE_{10} mode ($a = TE_{10}$) is given by

$$R_{TE_{10}} = -j\frac{\sqrt{8}Z_0}{\pi R(ab)^{1/2}\beta_c\beta_z}e^{-j\frac{\beta_0 b}{2}}\ \cos\left(\frac{\beta_0 b}{2}\right). \tag{4}$$

At high frequencies the coupling can be described by a diffraction model. Finally, the output of the crystal detector V_d, as viewed on a scope, is obtained from

$$\left(\frac{\partial}{\partial t} + \frac{1}{\tau}\right) V_d = \frac{k}{\tau} P_a(L,t), \tag{5}$$

where k characterizes the response of the crystal detector, and the time constant τ represents, *e.g.*, the bandwidth of the oscilloscope. The bits accumulated by a gated charge-sensitive analog-to-digital converter (GADC) are proportional to $\int_{t_1}^{t_2} dt\ V_d(t)$, with a gate width $(t_2 - t_1)$ of 50 ns. The Fourier transforms and integrations can be performed numerically. If several modes are included in the calculation, the effective voltage and current are sums over these modes, $\tilde{V}(z,\omega) = F(\omega)\sum_a \hat{\eta}_a\tilde{V}_a(z,\omega)$, and $\tilde{I}(z,\omega) = F(\omega)\sum_a \hat{\eta}_a\tilde{I}_a(z,\omega)$, where $\hat{\eta}_a$ denotes the relative coupling strength of mode a to the crystal detector as compared with the coupling of the TE_{10} mode ($\hat{\eta}_a$ is independent of ω, and $\hat{\eta}_{TE_{10}} = 1$). The power measured by the detector is simply $P(L,t) = I(L,t)V(L,t)$. An exact treatment must take into account the hybridization of degenerate modes due to wall losses [8].

During BLM commissioning it was found that monitor channel 3, detecting the RF power radiated above 21 GHz, provides the most useful signal, and all measurements reported in the following refer to this channel. The BLM signal is proportional to the square of the bunch charge and it decreases with increasing bunch length. To remove the dependence on the bunch charge, we normalize the signal by subtracting the GADC pedestal and dividing by the number of particles in units of 10^{10}. For example, at a nominal bunch population of $N_b = 4\times10^{10}$, a normalized signal of 10 corresponds to about 160 counts of the gated ADC, and the resolution limit due to digitization is about 0.6%.

In the SLC, one major source of IP bunch-length variation are changes in the linac injection phase, which are caused by thermal RF phase drifts. Such linac phase errors introduce a position-energy correlation along the bunch. The correlated energy spread then changes the IP bunch length via momentum compaction (R_{56}) in the 1.2-km long collider arcs. The BLM can be used to monitor and correct such changes. In Fig. 4 (left) we depict the measured and simulated BLM signal as a function of the linac injection phase. In the simulation, 10^4 particles were tracked in longitudinal phase space from the damping ring to the IP, and the beam power spectrum above 21 GHz was obtained by applying an FFT to the final distribution. Over the scan range considered, the simulated IP bunch length varies

by more than a factor of 3, with an associated dramatic change in the shape of the beam distribution. The source of the overall additive offset on the left axis is unclear. It could indicate high-frequency fine structure in the beam.

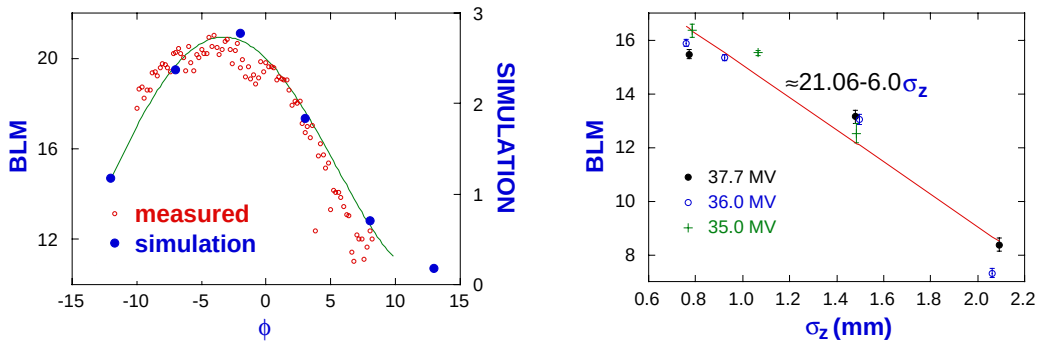

FIGURE 4. Left: BLM signal vs. linac injection time in degree S-Band, for $N_b \approx 1.2 \times 10^{10}$ with energy and RTL feedbacks active; each data point corresponds to one beam pulse; a simulation result (arbitrary units) is also shown. Right: calibration curve of BLM signal vs. rms IP bunch length; each data point derives from an average over 100 beam pulses, with rms variation shown by the error bars.

The BLM signal was calibrated by recording, over a few hundred pulses, both BLM signal and beam intensities for several different combinations of linac injection phase and compressor voltage. For each parameter setting, the beam energy profile at the end of the linac was also measured, using a wire scanner at a dispersive location. The corresponding IP distributions and bunch lengths were obtained from a multi-particle tracking simulation of the longitudinal beam transport. In the tracking, compressor voltage, compressor phase and the absolute offset of the linac phase were adjusted by fitting for optimum agreement between the simulated and measured energy profiles at the end of the linac [9]. The bunch compression, or anti-compression, in the arc was then calculated in a second simulation step, starting with the fitted end-of-linac distribution.

Figure 4 (right) shows the normalized BLM signal versus the simulated rms IP bunch length. The figure indicates that IP beam distributions with the same rms bunch length give rise to similar BLM signals. We attribute scatter in the data points to differences in the shape of the distributions for different compressor voltages, amounting to a 10% variation in rms bunch length.

From the measured fluctuation of the calibrated BLM signal we can estimate that the pulse-to-pulse rms bunch length variation is not larger than 5%.

BEAM-TIMING MONITOR

The relative timing of the two colliding electron and positron bunches can be determined from the microwave signals induced by the two beams in the same X-

Band waveguide as employed for bunch-length measurements. The relative phase between the two electromagnetic pulses travelling down the waveguide is sensitive to changes in the time delay between the arrival of the first beam (e^+) and the second beam (e^-) at the pickup. Jitter in the observed time delay is a direct measure of the jitter in the collision point.

The BTM setup is illustrated in the left picture of Fig. 5. The first bandpass filter has its center at 11.39 GHz, with full width of ± 50 MHz. The LO is a synthesizing signal generator, set to 11.49 GHz. Its stability, as measured with a frequency counter, is about ± 0.1 MHz, after thermal insulation. The output of the first mixer is passed through a 5% bandwidth filter tuned to 100 MHz. The filtered IF signal is passed through two amplifiers (47 dB gain, 2.4 dB NF, and 27 dB gain, 11 dB NF, respectively), and then split with a tee. One arm passes through a trombone phase-shifter permitting a full phase shift of 20° with a 0.002° dial indicator. The second arm passes through 38 meters of 3/8" Heliax cable, providing about 200 ns delay. The arms of the tee are passed through variable attenuators and combined in a second mixer. The final IF output is then low-pass filtered and can be viewed on a scope, saved to disk, or passed to a gated analog to digital converter for acquisition by the SLC control system. Figure 5 (right) shows typical signals measured after the first mixer and after the final low-pass filter.

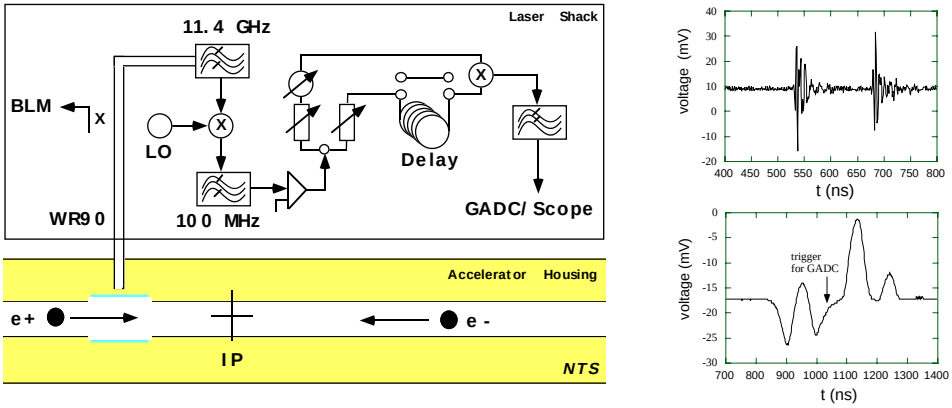

FIGURE 5. Left: schematic of BTM signal processing. Right: signal measured with crystal detector after the first mixer prior to second filter, where the signals induced by the two beams are clearly separated (top picture); and the low-pass filtered final two-beam signal after the 2nd mixer (bottom picture); the gate width of the GADC is 50 ns, and the trigger time (arrow) is chosen for a nominal signal close to zero.

We evaluate explicitly the limit in which the decay time of the output from the first filter is much less than the delay $(T_2 - T_1) \approx 300$ ns between the two bunches. We are considering then the time interval where the undelayed signal from the second bunch overlaps the delayed signal of the first bunch. The BTM scope waveform becomes $V_s(t) \approx kQ_1Q_2 \sin\theta$, with $k = |V_L|^2 \cos^2 \Psi$, where $|V_L|$ denotes the voltage of the local oscillator, and $\Psi = \arctan(Q(\omega_{IF}/\omega_2 - \omega_2/\omega_{IF})$, with $Q =$

$2\omega_2/\nu_2$ the quality factor of the second (narrow-band) filter, ω_2 its center frequency, and $\omega_{IF} = (\omega_1 - \omega_L)$ the intermediate frequency which is obtained by mixing the signal after the first filter, centered around ω_1, with the local oscillator signal of frequency ω_L. The variables Q_1 and Q_2 are the charges of the two bunches, and the relative beam phase θ is $\theta \equiv (\omega_1 \Delta T - \omega_{IF} T_D - \phi + \pi/2)$, where ΔT is the arrival time difference, whose fluctuation we want to measure, and T_D the delay time of the cable. The phase ϕ is a constant. Whatever the nominal beam delay $\Delta T = (T_2 - T_1)$ may be, using a phase shifter one may adjust ϕ to put the scope signal at a null. In this case, maximum sensitivity is attained and the nominal relative beam phase is 0. For small variations, one has $V_s(t) \approx k Q_1 Q_2 \theta$, and jitter in relative beam timing then correlates linearly with $V_s/(Q_1 Q_2)$. The counts registered in a gated analog-to-digital converter are given by $\int_{T_{trig}}^{T_{trig}+T_{gate}} dt\ V_s(t)$, up to an overall constant. The trigger time is T_{trig} and the gate width T_{gate} is 50 ns. Thus, in practice, adjusting ϕ also requires a choice of gate position. A refined numerical model of the signal waveforms has also been developed, taking into account the filter characteristics as measured with the network analyzer, and the numerically computed waveforms incident on the first filter (including the dispersion characteristics of the waveguide). Signals predicted by this model are in reasonable agreement with the measurement.

The raw signal is normalized by first subtracting the pedestal and then dividing by the product of the e^+ and e^- intensities (particles per bunch in units of 10^{10}). The two calibration curves in Fig. 6 show the BTM signal as a function of the delay (in units of degree X-Band) in one of the two arms, which was varied using the phase trombone. The left picture is an autophase measurement (one beam only, delay cable removed); the right is an actual two-beam measurement (with delay cable). Using the fitted slope we can convert the measured signal changes into degree X-Band or time. The much larger scattering of the data in the right picture represents real beam-timing jitter, as large as 14° X-Band peak to peak, or 5° rms.

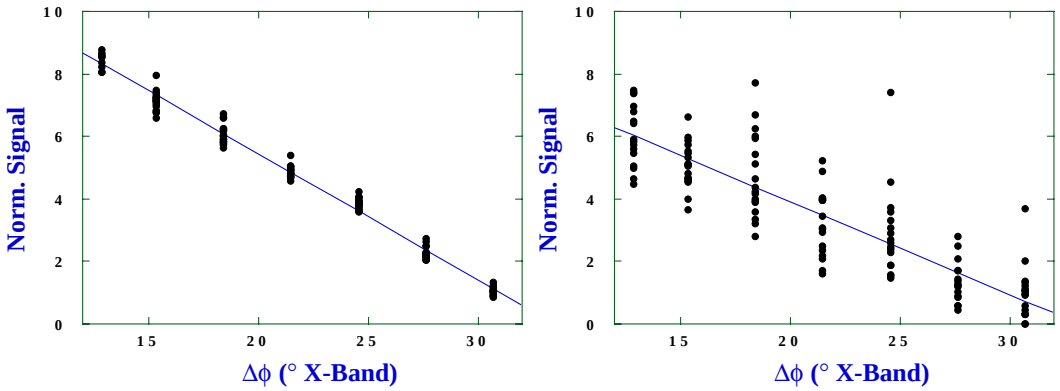

FIGURE 6. Calibration measurements: normalized timing-monitor signal versus the trombone phase difference in degree X-Band; (left) signal for one beam with cable delay removed; (right) signal for two beams including cable delay.

We have also measured the BTM signal as a function of the electron-beam energy at the end of the linac, holding the energy of the positron beam constant. From this measurement and from the phase calibration performed at the same time, we estimate the momentum compaction of the SLC North arc as $R_{56} \approx 120$ mm, not too far from the theoretical value (145 mm).

CONCLUSION

The RF BLM in the SLC South Final Focus monitors pulse-to-pulse changes in the IP bunch length of both colliding beams, with a precision of a few percent. Its response to linac injection time and compressor voltage is consistent with simulations of the longitudinal beam transport. The bunch length was found to be stable to within 5% and, thus, it is not a dominant source of pulse-to-pulse fluctuation in luminosity or beamstrahlung. The RF BTM detects changes in the relative arrival time of electron and positron bunches at the SLC interaction point, with a short-term resolution better than 5° X-Band. Our measurement results indicate a luminosity degradation due to beam timing jitter of the order of 2%.

ACKNOWLEDGEMENTS

We thank M. Ross, M. Breidenbach and N. Phinney for support, A. Menegat, S. Tantawi and S. Hanna for helpful advice, M. Woods for sharing the laser shack with us, and H. Rogers for installing the BLM shielding box.

REFERENCES

1. K. Yokoya and P. Chen, "Beam-beam phenomena in linear colliders", *Lecture at 1990 US-CERN School on Particle Accelerators, Hilton Head Island* (1990).
2. D. Schulte, "Study of Electromagnetic and Hadronic Background in the Interaction Region of the TESLA Collider", Ph.D. thesis, University of Hamburg (1996).
3. E. Babenko, R.K. Jobe, D. McCormick, J.T. Seeman, "Length Monitor for 1 mm SLC Bunches", *Proc. of IEEE PAC93, Washington*, p. 2423 (1993).
4. J.D. Lawson, "Radiation from a Ring Charge Passing Through a Resonator", Rutherford Lab. Report *RHEL/M* **144** (1968), *Particle Accelerators* **25**, 107 (1990).
5. K. Bane, M. Sands, "Wakefields of Very Short Bunches in an Accelerating Cavity", *Particle Accelerators* **25**, 73 (1990)
6. "MAFIA RELEASE 3", *DESY* **M-90-05K** (1990).
7. R.E. Collin, "Foundations for Microwave Engineering", McGraw-Hill (1966).
8. K. Kurokawa, "Electromagnetic Waves in Waveguides with Wall Impedance", *IRE Trans. Microwave Theory and Techniques*, p. 314 (1962).
9. K.L.F. Bane, F.-J. Decker, J.T. Seeman, F. Zimmermann, "Measurement of the Longitudinal Wakefield and the Bunch Shape in the SLAC Linac", *Proc. of IEEE PAC 97, Vancouver*, and *SLAC-PUB*-**7536** (1997).